J|A|C|S ARTICLES

Published on Web 01/09/2009

# Nonaromatic Core−Shell Structure of Nanodiamond from Solid-State NMR Spectroscopy

XiaoWen Fang,[†] JingDong Mao,[‡] E. M. Levin,[§,||] and Klaus Schmidt-Rohr*[,†,§]

*Department of Chemistry, Iowa State University, Ames, Iowa 50011, Department of Chemistry and Biochemistry, Old Dominion University, Norfolk, Virginia 23529, Ames Laboratory DOE, Ames, Iowa 50011, and Department of Physics and Astronomy, Iowa State University, Iowa 50011*

Received July 12, 2008; E-mail: srohr@iastate.edu

***Abstract:*** The structure of synthetic nanodiamond has been characterized by $^{13}C$ nuclear magnetic resonance (NMR) spectral editing combined with measurements of long-range $^{1}H-^{13}C$ dipolar couplings and $^{13}C$ relaxation times. The surface layer of these ∼4.8-nm diameter carbon particles consists mostly of $sp^3$-hybridized C that is protonated or bonded to OH groups, while $sp^2$-hybridized carbon makes up less than 1% of the material. The surface protons surprisingly resonate at 3.8 ppm, but their direct bonding to carbon is proved by fast dipolar dephasing under homonuclear decoupling. Long-range $^{1}H-^{13}C$ distance measurements, based on $^{13}C\{^{1}H\}$ dipolar dephasing by surface protons, show that seven carbon layers, in a shell of 0.63 nm thickness that contains ∼60% of all carbons, predominantly resonate more than +8 ppm from the 37-ppm peak of bulk diamond (i.e., within the 45−80 ppm range). Nitrogen detected in $^{15}N$ NMR spectra is mostly not protonated and can account for some of the high-frequency shift of carbon. The location of unpaired electrons (∼40 unpaired electrons per particle) was studied in detail, based on their strongly distance-dependent effects on $T_{1,C}$ relaxation. The slower relaxation of the surface carbons, selected by spectral editing, showed that the unpaired electrons are not dangling bonds at the surface. This was confirmed by detailed simulations, which indicated that the unpaired electrons are mostly located in the disordered shell, at distances between 0.4 and 1 nm from the surface. On the basis of these results, a nonaromatic core−shell structural model of nanodiamond particles has been proposed.

## Introduction

Nanodiamond, consisting mostly of crystalline balls of a few thousand carbon atoms with some nitrogen, oxygen, and hydrogen, is a fascinating synthetic material with many promising properties.[1−4] It has also been found in nature, in particular in carbonaceous meteorites[5−8] and in terrestrial rocks in the vicinity of the K/T boundary.[9] While many types of nanocrystalline diamond have been described in the literature (for a good review, see ref 2), most commercial nanodiamond is produced as a bulk material by detonation from carbon-containing precursors such as TNT and hexogen, which after separation from graphitic soot results in nanodiamond with ∼2% nitrogen and ∼1 wt % (∼10 at. %) hydrogen.[1,2,10] This "ultradispersed diamond" is synthesized in quantities of hundreds of kilograms, for wear-resistant metal-composite coatings, filled elastomers with improved properties, and lubricants,[1,2] and with potential applications in drug delivery,[4] protein purification,[11] catalysis,[12] as fluorescent markers for cell imaging,[13] as well as nucleation centers for the growth of diamond films.[14]

While the diameter of the crystalline core in detonation nanodiamond is found consistently between 4 and 5 nm,[2,15−17] their surface and core−shell structure is still a matter of an ongoing debate. In terms of chemical reactivity and interparticle interactions, the composition of the surface is clearly most important. [4] Do they have a fullerenic ("bucky-diamond"[18,19]), onion-shell, or disordered graphitic surface as has been widely

[†] Department of Chemistry, Iowa State University.
[‡] Old Dominion University.
[§] Ames Laboratory DOE.
[||] Department of Physics and Astronomy, Iowa State University.

(1) Dolmatov, V. Y. *Russ. Chem. Rev.* **2001**, *70*, 607–626.
(2) Shenderova, O. A.; Zhirnov, V. V.; Brenner, D. W. *Crit. Rev. Solid State Mater. Sci.* **2002**, *27*, 227–356.
(3) Baidakova, M.; Vul, A. Y. *J.Phys. D: Appl. Phys.* **2007**, *40*, 6300–6311.
(4) Krueger, A. *J. Mater. Chem.* **2008**, *18*, 1485–1492.
(5) Lewis, R. S.; Anders, E.; Draine, B. T. *Nature* **1989**, *339*, 117–121.
(6) Daulton, T. L.; Eisenhour, D. D.; Bernatowicz, T. J.; Lewis, R. S.; Buseck, P. R. *Geochim. Cosmochim. Acta* **1996**, *60*, 4853–4872.
(7) Cody, G. D.; Alexander, C. M. O. D.; Tera, F. *Geochim. Cosmochim. Acta* **2002**, *66*, 1851–1865.
(8) Cody, G. D.; Alexander, C. M. O. D. *Geochim. Cosmochim. Acta* **2005**, *69*, 1085–1097.
(9) Gilmour, I.; Russell, S. S.; Arden, J. W.; Lee, M. R.; Franchi, I. A.; Pillinger, C. T. *Science* **1992**, *258*, 1624–1626.
(10) Donnet, J. B.; Fousson, E.; Delmotte, L.; Samirant, M.; Baras, C.; T.-K., W.; Eckhardt, A. *Phys. Theor. Chem.* **2000**, *3*, 831–838.
(11) Bondar, V. S.; Pozdnyakova, I. O.; Puzyr, A. P. *Phys. Sol. State* **2004**, *46*, 758–760.
(12) Bogatyreva, G. P.; Marinich, M. A.; Ishchenko, E. V.; Gvyazdovskaya, V. L.; Bazalii, G. A.; Oleinik, N. A. *Phys. Solid State* **2004**, *46*, 738–741.
(13) Yu, S.-J.; Kang, M.-W.; Chang, H.-C.; Chen, K.-M.; Yu, Y.-C. *J. Am. Chem. Soc.* **2005**, *127*, 17604–17605.
(14) Vul', A. Y.; Golubev, V. G.; Grudinkin, S. A.; Krueger, A.; Naramoto, H. *Phys. Astron.* **2002**, *28*, 787–789.
(15) Badziag, P.; Verwoerd, W. S.; Ellis, W. P.; Greiner, N. R. *Nature* **1990**, *343* (18), 244–245.
(16) Raty, J. Y.; Galli, G. *Nat. Mater.* **2003**, *2*, 792–795.
(17) Wang, C.; Chen, J.; Yang, G.; Xu, N. *Angew. Chem., Int. Ed.* **2005**, *44*, 7414–7418.
(18) Barnard, A. S.; Sternberg, M. *J. Phys. Chem. B* **2005**, 17107–17112.

 **10.1021/ja8054063 CCC: $40.75** 

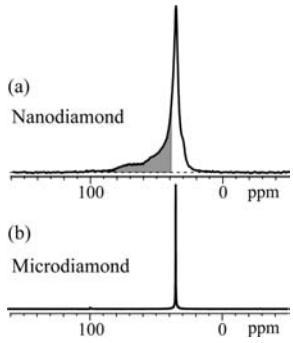


***Figure 1.*** Quantitative direct-polarization $^{13}C$ NMR spectra of (a) nanodiamond and (b) microdiamond, measured at 14 and 6.5 kHz MAS, respectively. A Hahn echo was used before detection for obtaining perfect baselines. The highest peaks at 37 ppm in both spectra represent the carbon signals from crystalline diamond. The signal in the shaded range in (a), between ~40 and 85 ppm, must be assigned to disordered carbon in nanodiamond.

concluded or assumed,[20−26] is there an amorphous graphitic component,[27−29] or are they fully $sp^3$-hybridized with a hydrogenated surface?[2,29] Are there dangling bonds at the surface? [25] Are there many OH groups at the diamond surface,[30,31] or is the O−H vibration in Raman spectroscopy just from adsorbed water?[29] Is the nitrogen at the surface or in the core?[18,32] The structure of the diamond surface also has major effects on friction[30,31] and surface conductivity.[33,34]

Further, why is the diameter of the crystalline core between 4 and 5 nm quite independent of synthesis conditions?[1,15,21,27,32] Is the interior hollow?[22] Is the diamond lattice distorted, and if so, why?[21] How common are defects, and how stable is the interior of the particles?[35] What is the origin of the broad high-frequency "foot" in the $^{13}C$ spectrum, see Figure 1a?[10,25]

Many of these questions can be addressed by nuclear magnetic resonance (NMR) spectroscopy, relaxation-time, and internuclear-distance measurements. Previous studies have touched on some of these issues,[7,10,25,36] but we will show that important spectral features have not been attributed correctly and several proposed conclusions have to be revised. For instance, in some cases, only a single sharp $^{13}C$ NMR resonance was reported, overlooking the high-frequency components shown shaded in Figure 1, which account for nearly half the spectral area; this may result in significant underestimates of nanodiamond abundance based just on the sharp peak, for instance in meteorite organic matter. Crucial new insights are provided by $^1H-^{13}C$ distance measurements and quantitative analyses of the nuclear relaxation produced by unpaired electron spins, which had not been performed before.

The quantitative $^{13}C$ NMR spectrum in Figure 1a shows that about half of the carbon resonates in broad bands to the left of the main diamond resonance at 37 ppm but signals of $sp^2$-hybridized carbons are negligible. Our studies further reveal that nanodiamond exhibits other unusual NMR properties such as an unexpected $^1H$ chemical shift. We have applied spectral-editing techniques in addition to quantitative $^{13}C$ NMR to characterize the surface and subsurface composition of nanodiamond, including a sample annealed at 600 °C in an argon atmosphere. Based on $^1H-^{13}C$ long-range dipolar dephasing, it is shown that the carbons resonating at higher frequency form a disordered shell. Its thickness is estimated on the basis of spectrally resolved $^{13}C\{^1H\}$ HARDSHIP NMR dephasing. Strong effects of unpaired electrons on longitudinal ($T_{1,C}$) relaxation times[25] of $^{13}C$ nuclei have now been observed with spectral resolution, revealing slower relaxation of surface carbons. Specifically, the distance of the unpaired electrons from the surface and core of the particles is estimated by quantitative analysis of $T_{1,C}$ relaxation. On this basis, a relatively detailed model of the nonaromatic core−shell structure of nanodiamond is proposed.

## Experimental Section

**Materials.** Nanodiamond (97% purity) and microdiamond (natural monocrystalline powder, ca. 1 $\mu$m size, 99.9% purity) were purchased from Sigma-Aldrich and used without any additional chemical treatments. In order to study structural changes after annealing, the nanodiamond was heated at 600 °C for 3 h under an argon atmosphere. Another nanodiamond sample of somewhat lower purity (95%) was also studied and gave similar results (not shown here).

**Elemental Analysis.** After freeze-drying the sample overnight, a triplicate measurement of C, H, and N concentrations was performed using a Perkin-Elmer Series II Analyzer 2400. The instrumental precision is within 0.3%.

**Wide-Angle X-ray Diffraction.** Wide-angle X-ray diffraction (WAXD) experiments were conducted to estimate the diameter of the crystalline core of the nanodiamond particles. The samples were placed in plastic or quartz sample holders, which allows us to propose a simple explanation for a band around $2\theta = 13°$ reported in ref 20. A microdiamond sample was also measured for reference.

**NMR Spectroscopy.** Most of the NMR experiments were performed using a Bruker DSX400 spectrometer at 400 MHz for $^1H$ and 100 MHz for $^{13}C$. A Bruker 4-mm double-resonance magic-angle spinning (MAS) probe head was used for the 13- and 14-kHz MAS experiments, while the 6.5-kHz MAS experiments were performed with larger 7-mm sample rotors in a 7-mm Bruker double-resonance probe head.

**High-speed quantitative $^{13}C$ DP/MAS NMR.** Quantitative $^{13}C$ DP/MAS (direct polarization/magic angle spinning) experiments were run at a spinning speed of 14 kHz with TPPM decoupling of

(19) Raty, J. Y.; Galli, G.; Bostedt, C.; Buuren, V. T. W.; Terminello, L. J. *Phys. Rev. Lett.* **2003**, *90*, 0374011−0374014.
(20) Aleksenskii, A. E.; Baidakova, M. V.; Vul, A. Y.; Siklitskii, V. I. *Phys. Solid State* **1999**, *41*, 668–671.
(21) Shames, A. I.; Panich, A. M.; Kempinski, W.; Alexenskii, A. E.; Baidakova, M. V.; Dideikin, A. T.; Osipov, V. Y.; Siklitski, V. I.; Osawa, E.; Ozawa, M.; Vul, Y. A. *J. Phys. Chem. Solids* **2002**, *63*, 1993–2001.
(22) Vereshchagin, A. L.; Yur'ev, G. S. *Inorg. Mater.* **2003**, *39*, 247–253.
(23) Dement'ev, A. P.; Maslakov, K. I. *Phys. Solid State* **2004**, *46*, 678–680.
(24) Raty, J. Y.; Galli, G. *J. Electroanal. Chem.* **2005**, *584*, 9–12.
(25) Panich, A. M.; Vieth, H. M.; Osawa, E.; Takahashi, M.; Vul, Y. A. *Eur. Phys. J. B.* **2006**, *52*, 397–402.
(26) Barnard, A. S.; Sternberg, M. *J. Mat. Chem.* **2007**, *17*, 4811–4819.
(27) Baidakova, M. V.; Vul, A. Y.; Siklitski, V. I.; Faleev, N. N. *Phys. Solid State* **1998**, *40*, 715–718.
(28) Chen, J.; Deng, S. Z.; Chen, J.; Yu, Z. X.; Xu, N. S. *Appl. Phys. Lett.* **1999**, *74*, 3651–3653.
(29) Osawa, E. *Diamond Relat. Mater.* **2007**, *16*, 2018–2022.
(30) Qi, Y.; Konca, E.; Alpas, A. T. *Surf. Sci.* **2006**, *600*, 2955–2965.
(31) Konicek, A. R.; Grierson, D. S.; Gilbert, P. U. P. A.; Sawyer, W. G.; Sumant, A. V.; Carpick, R. W. *Phys. Rev. Lett.* **2008**, *100*, 235502.
(32) Krueger, A.; Kataoka, F.; Ozawa, M.; Fujino, T.; Suzuki, Y.; Aleksenskii, A. E.; Vul, A. Y.; Osawa, E. *Carbon* **2005**, *43*, 1722–1730.
(33) Andriotis, A. N.; Mpourmpakis, G.; Richter, E.; Menon, M. *Phys. Rev. Lett.* **2008**, *100*, 206801.
(34) Hirama, K.; Takayanagi, H.; Yamauchi, S.; Yang, J. H.; Kawarada, H.; Umezawa, H. *Appl. Phys. Lett.* **2008**, *92*, 112107.
(35) Duijvestijn, M. J.; Van, D. L. C.; Smidt, J.; Wind, R. A.; Zilm, K. W.; Staplin, D. C. *Chem. Phys. Lett.* **1983**, *102*, 25–28.
(36) Alam, T. M. *Mater. Chem. Phys.* **2004**, *85*, 310–315.

$^1$H. For dead-time free detection that ensures good spectral baselines, an exorcycled[37] 180° pulse was applied after a rotation period $t_r$, which generates a Hahn echo at time $2t_r$. The 90° $^{13}$C pulse length was 4 $\mu$s. Recycle delays were tested by the CP/$T_1$/TOSS technique to make sure that all carbon sites are fully relaxed. The details of this technique have been described elsewhere.[38] In order to obtain quantitative information on nonprotonated carbons, DP/MAS $^{13}$C NMR spectra were acquired under the same conditions with a dipolar dephasing time of 68 $\mu$s.[39] Chemical shifts were referenced to carboxyl resonance of glycine at 176.49 ppm. In order to see the presence of sidebands of the sample, $^{13}$C DP/MAS spectra were also measured on a Bruker 600-MHz NMR spectrometer, with 2-s recycle delays at 0-, 12-, and 14-kHz MAS; these were the only spectra not recorded at 9.4 T. In order to look for signals of sp$^2$-hybridized carbons, direct polarization experiments with four-pulse total suppression of sidebands (TOSS)[40] were also performed at spinning frequencies of 13 and 6.5 kHz, using 4- and 7-mm diameter rotors, respectively, with recycle delays of 4 s in order to maximize the signal-to-noise ratio, and of 400 s in order to ensure detection of potential long-$T_1$ sp$^2$-hybridized carbons.

**$^1$H NMR Probehead Background Suppression.** One-dimensional solid-state $^1$H NMR spectra were recorded at 0, 6.5, and 30 kHz. Probe-head background signal was suppressed by the simple and reliable scheme of ref 41. In short, two one-pulse spectra, with pulse flip angles of $\beta$ and $2\beta$ (e.g., 90° and 180°), are acquired. The essentially background-free spectrum is obtained by subtracting the second spectrum, scaled by 0.5, from the first. Chemical shifts were referenced to water at 4.9 ppm.

**Spectral Editing of Protonated Carbons ($CH_2$ + CH).** The spectrum of carbons bonded to H can be obtained with good sensitivity based on cross-polarization and dipolar dephasing.[42] Two spectra are recorded. The first one is a CP/TOSS spectrum with a short CP contact time of 0.2 ms; the second one is a CP/TOSS spectrum with the same CP contact time but 40-$\mu$s dipolar dephasing. The first spectrum is predominantly that of protonated carbons, but residual peaks of quaternary carbons result from two-bond magnetization transfer. The second one contains only the residual signals of quaternary carbons or mobile segments. The difference of these spectra is the spectrum of the $CH_2$ and CH carbons.

**CH Spectral Editing.** For CH selection, the robust dipolar DEPT method based on C−H multiple-quantum coherence was used.[43] CH-group multiple-quantum coherence is not dephased by the spin-pair CH dipolar coupling, while $CH_2$ group coherence is dephased by the dipolar coupling of the carbon to the second proton. The first of a pair of spectra recorded contains signals of CH, as well as residual quaternary-carbon peaks. The latter are removed by taking the difference with a second spectrum acquired with the same pulse sequence, except for additional 40-$\mu$s dipolar dephasing before detection. [43] The spinning frequency was 5.787 kHz.

**Two-Dimensional $^1$H−$^{13}$C NMR.** Two-dimensional (2D) $^1$H−$^{13}$C wide-line separation (WISE) and heteronuclear correlation (HetCor) NMR experiments with frequency-switched Lee−Goldburg (FSLG) homonuclear decoupling during the evolution time was performed at a spinning speed of 6.5 kHz. Lee−Goldburg cross polarization (LG-CP) of 0.1 ms was used to suppress $^1$H−$^1$H spin diffusion during polarization transfer and show mostly one-bond $^1$H−$^{13}$C connectivity.

**$^{15}$N NMR.** Direct-polarization $^{15}$N NMR experiments were run at 6.5 kHz MAS with 1-s recycle delays. A $^{15}$N 180° pulse of 18.4 $\mu$s duration at $t_r$ was used to generate a Hahn echo at $2t_r$ for dead-time-free detection. Recoupled dipolar dephasing was achieved by switching $^1$H decoupling off during the $2t_r$ period around the 180° pulse and applying $^1$H 180° pulses at $t_r$/2 and $3t_r$/2. In total, 780 000 scans were averaged. Chemical shifts were referenced to liquid ammonia at 0 ppm.

**Long-Range C−H REDOR.** The signals of nonprotonated carbons near the surface, detected via CP/TOSS from surface protons followed by gated decoupling, can be distinguished efficiently from interior carbons, detected via DP/TOSS/gated decoupling, using recoupled dipolar dephasing (REDOR), with two 8-$\mu$s $^1$H 180° pulses per rotation period that prevent MAS from averaging out weak CH dipolar couplings.[44] The spinning frequency was 14 kHz.

**Dip-Shift NMR with Dipolar-Dephasing Difference.** In order to identify C directly bonded to H, the strongly distance-dependent $^{13}$C−$^1$H dipolar coupling was estimated by "dip-shift" NMR,[45,46] where the C−H dipolar coupling strength is probed in terms of the dephasing of the $^{13}$C signal under the influence of the $^1$H nuclear magnet, with homonuclear dipolar decoupling of $^1$H by MREV-8[47] for a time $t_{MREV}$ during the time period $t_r$ before a 180° pulse generating a Hahn echo. In nanodiamond, overlap of signals of the abundant interior carbons with those of the surface carbons is a problem. Since the surface carbons are closest to protons, their signal can be enhanced by using a short $^1$H−$^{13}$C cross-polarization time of 0.1 ms.

Nevertheless, signal of nonprotonated C contributed about one-fourth of the total intensity. In order to remove this overlapping signal, the same experiment was run with 40 $\mu$s of dipolar dephasing before detection, centered on a time $1.5t_r$ from the start of signal evolution ($0.5t_r$ before the start of detection). Scaling this signal up by a factor 1.11 to correct for two-bond C−H dephasing and subtracting it from the full spectrum leaves only the signal of protonated C, as confirmed by applying this "dipolar dephasing difference" experiment to a model compound, alanine. The experiments were performed at a spinning frequency of 4 kHz.

**$^{13}$C{$^1$H} HARDSHIP NMR.** $^{13}$C{$^1$H} HARDSHIP (*H*eteronucle*A*r *R*ecoupling with *D*ephasing by *S*trong *H*omonuclear *I*nteractions of *P*rotons) experiments[48] were performed at 6.5 kHz MAS in order to quantify the diameter of nanodiamond particles and the thickness of the disordered shell more accurately. This approach is based on the strongly distant-dependent dipolar couplings between the protons in the surface layer and $^{13}$C-nuclei in the inner layers. The $CH_n$ multispin dynamics of HARDSHIP are more tractable than those in the corresponding REDOR experiments, since $^1$H−$^1$H dipolar couplings do not significantly affect the $^1$H−$^{13}$C dephasing during HARDSHIP.[48]

**$^{13}$C $T_1$ Relaxation Measurements and Simulations.** The $^{13}$C $T_1$ relaxation behavior was measured by CP/ or DP/$T_1$-TOSS[49] at 6.25 kHz MAS combined with spectral editing techniques, such as selection of protonated carbons or long-range C−H dipolar dephasing after direct polarization, to obtain the $T_1$ values of different types of carbons. The recovery times varied from 1 to 2000 ms. The recycle delay was 10 s. For reference, the $T_1$ relaxation times of synthetic and of natural microdiamonds were also measured, using saturation recovery with TOSS detection and recovery delays of 1−2000 s.

(37) Bodenhausen, G.; Freeman, R. *J. Magn. Reson.* **1977**, *28*, 471–476.
(38) Mao, J.-D.; Hu, W.-G.; Schmidt-Rohr, K.; Davies, G.; Ghabbour, E. A.; Xing, B. *Soil Sci. Soc. Am. J.* **2000**, *64*, 873–884.
(39) Mao, J.-D.; Schmidt-Rohr, K. *Environ. Sci. Technol.* **2004**, *38*, 2680–2684.
(40) Dixon, W. T. *J. Chem. Phys.* **1982**, *77*, 1800–1809.
(41) Chen, Q.; Hou, S.-S.; Schmidt-Rohr, K. *Solid State Nucl. Magn. Reson.* **2004**, *26* (1), 11–15.
(42) Wu, X.; Burns, S. T.; Zilm, K. W.; Spectral editing in CPMAS, N. M. R. *J. Magn. Reson., A* **1994**, *111*, 29–36.
(43) Schmidt-Rohr, K.; Mao, J.-D. *J. Am. Chem. Soc.* **2002**, *124*, 13938–13948.
(44) Mao, J.-D.; Schmidt-Rohr, K. *J. Magn. Reson.* **2003**, *162*, 217–227.
(45) Munowitz, M. G.; Griffin, R. G.; Bodenhausen, G.; Huang, T. H. *J. Am. Chem. Soc.* **1981**, *103*, 2529–2533.
(46) Schaefer, J.; McKay, R. A.; Stejskal, E. O.; Dixon, W. T. *J. Magn. Reson.* **1983**, *52*, 123–129.
(47) Rhim, W.-K.; Elleman, D. D.; Vaughan, R. W. *J. Chem. Phys.* **1973**, *59*, 3740–3749.
(48) Schmidt-Rohr, K.; Rawal, A.; Fang, X. W. *J. Chem. Phys.* **2007**, *126*, 0547011−05470116.
(49) Torchia, D. A. *J. Magn. Reson.* **1978**, *30*, 613–616.

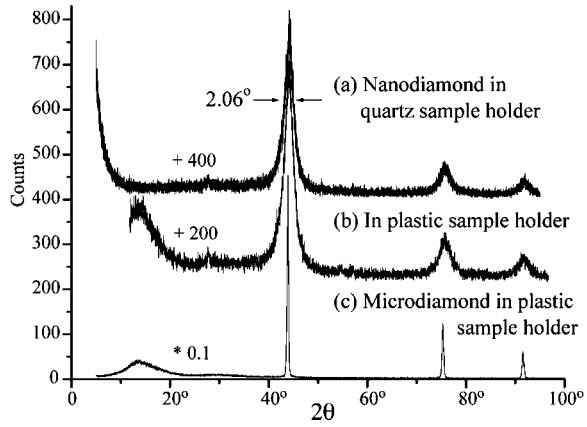


***Figure 2.*** WAXD pattern of (a, b) nanodiamond and (c) microdiamond powder, conducted with the sample in (a) a quartz or (b, c) plastic sample holder. For clarity, intensity patterns of (a) and (b) were vertically shifted by 400 and 200 counts, respectively, while the intensity in (c) was scaled down 10 times.

$T_1$ relaxation curves were simulated in full detail in a model 4.8-nm diameter sphere made up of 24 carbon layers spaced by 0.1 nm, with a lateral C−C spacing of 0.2 nm. Relaxation was generated by 35−40 unpaired electrons distributed randomly within a specified range of depths from the particle surface, with rates of $1/T_{1,C} = ((1/3.5s)/nm^6)\sum_{n_{electron}} 1/r_n^6$, where $r_n$ is the distance between a given carbon and the $n$th unpaired electron. Carbons within a certain range (typically 0.3 nm) from the unpaired electrons were treated as unobservable (see details below). Each sphere was surrounded by six neighboring spheres with the same distribution of unpaired electrons.

## Results and Discussion

After a brief generic characterization of the nanodiamond sample by $^{13}$C NMR and WAXD, we will first prove that the nanodiamond surface is mostly protonated and hydroxylated, then describe measurements of depth from this protonated surface, and finally characterize the interior in more detail, focusing on the location of unpaired electrons in the nanodiamond, based on their effects on nuclear relaxation.

**Quantitative, Unselective $^{13}$C NMR.** Figure 1 shows quantitative $^{13}$C NMR spectra of nanodiamond and microdiamond, obtained with 90°-pulse excitation and a Hahn echo after 5- and 1000-s recycle delays, respectively, at 13 and 6.5 kHz MAS. We observe a sharp, narrow peak at 37 ppm in the microdiamond spectrum, which is assigned to the diamond core. In contrast, the chemical shift range of nanodiamond is very broad, from 20 to 85 ppm, with an asymmetric broad high-frequency wing from 40 to 85 ppm. The main band around 37 ppm arises mostly from the nanodiamond core, while the asymmetric broad wing must be assigned to disordered layers close to the surface, as will be shown by $^1$H−$^{13}$C dephasing below.

**WAXD.** The WAXD pattern of nanodiamond powder is shown in Figure 2. It shows the broadening of the Bragg peaks characteristic of detonation nanodiamond.[20] Data obtained in a quartz and a plastic sample holder are compared in the figure. The latter shows a broad reflection near 13°, similar to those reported previously for nanodiamond and interpreted in terms of a surface structure containing many sp$^2$-hybridized carbons.[20] However, the absence of this band in the data obtained with the quartz sample holder reveals it to be an artifact.

In spherical nanocrystals, a finite crystal diameter $L$ results in a broadening $\Delta\theta$ of a given Bragg reflection at scattering angle $\theta$, according to the Scherrer equation

$$L = \frac{0.9\lambda}{\beta_{1/2}\cos\theta} \quad (1)$$

where $\beta_{1/2}$ is the full width at half maximum of the peak and $2\theta$ is the diffraction angle. Analysis of the peaks in Figure 2 gives a diameter of the crystalline core of 4.1 ± 0.2 nm in our sample.

**Elemental Analysis.** Elemental analysis yields C/H/N atomic ratios of 100:14:2. The uncertainty of the C and H abundances is ±1, mostly due to the likely presence of residual adsorbed water.

**Search for sp$^2$-Hybridized C.** The quantitative $^{13}$C spectrum in Figure 1 shows no apparent peaks in the >100 ppm region, where sp$^2$-hybridized carbons resonate. In order to ensure that we do not overlook long-$T_{1,\ C}$ sp$^2$-hybridized carbons, we acquired a spectrum with 400-s recycle delay and total suppression of sidebands at 6.5-kHz MAS in a 7-mm rotor, see Figure 3a. No signals from sp$^2$ carbons are observed. We can also look for such sites with a 4-s recycle delay and many more scans in a 4-mm rotor at 13 kHz MAS, and in a larger 7-mm rotor at 6.5 kHz MAS with TOSS. In the resulting spectra shown in Figure 3b,c, we observe only residual spinning sidebands at ~175 ppm. The intensity, which could be from one of MAS sidebands of alkyl carbons at 37 ppm due to the large paramagnetic shift anisotropies (see details below), accounts for less than 1% of all carbons.

By contrast, Panich et al.[25] reported a peak at ~111 ppm, which they attributed to aromatic surface sites. The position of

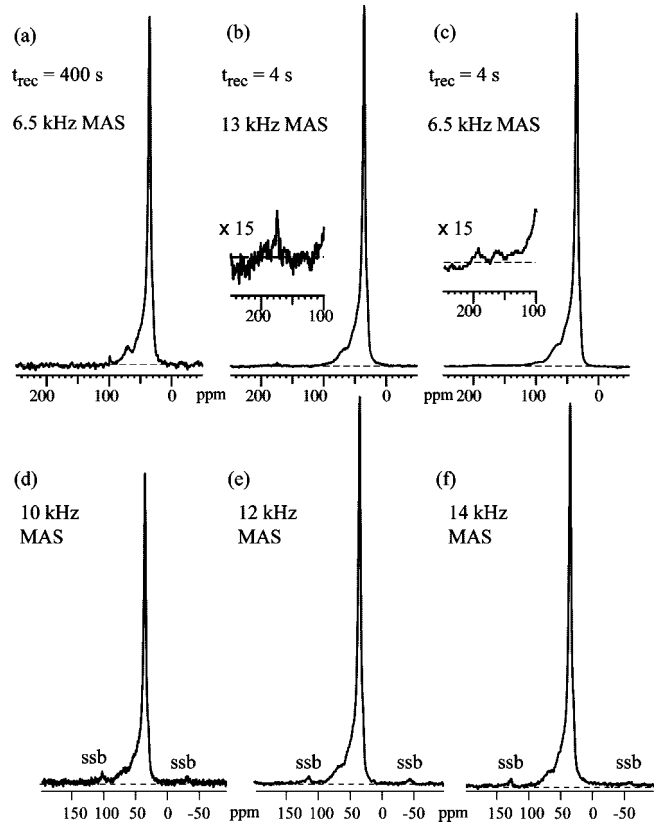


***Figure 3.*** (a−c) Search for graphitic or other sp$^2$-hybridized carbon signals in quantitative DP/TOSS $^{13}$C NMR spectra, with 400 (at 6.5 kHz MAS) and 4 s (at 13 and 6.5 kHz MAS) recycle delays, for full relaxation and maximum sensitivity, respectively. The insets in (b) and (c) show the region from 100 to 250 ppm enlarged 15 times; less than 1% of carbon could be sp$^2$ carbon or could be a spinning-sideband signal. (d−f) DP/MAS $^{13}$C NMR spectra taken at 150 MHz (in a field of 14.1 T) at 10, 12, and 14 kHz MAS. They clearly show side bands from the highest alkyl carbon peak.

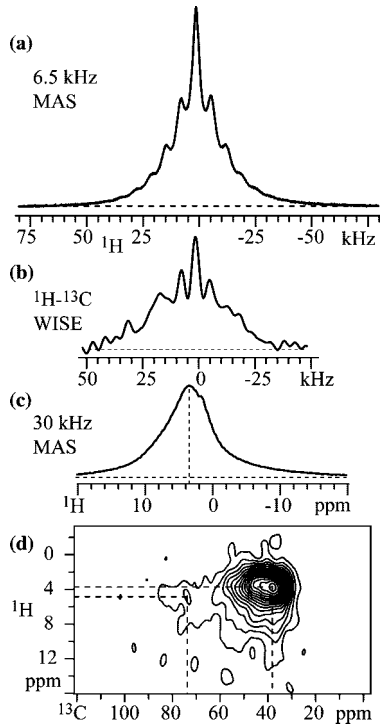


***Figure 4.*** $^{1}$H spectra of nanodiamond: (a) One-dimensional spectrum at slow (6.5-kHz) MAS, with background suppression. (b) $^{1}$H projection from a 2D $^{13}$C−$^{1}$H wide line separation spectrum taken at 6.5 kHz MAS. (c) 30-kHz MAS spectrum, with background suppression. (d) 2D $^{13}$C−$^{1}$H HetCor spectrum taken at 6.5 kHz MAS.

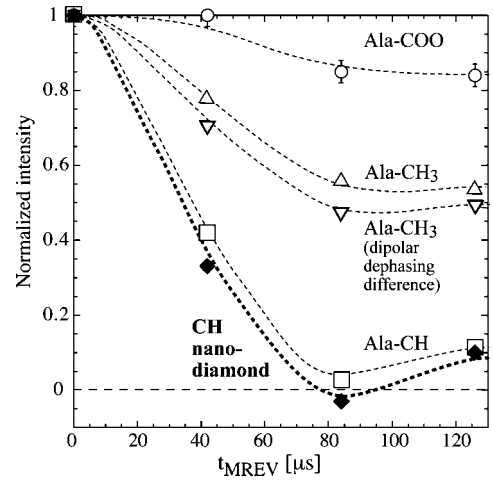


***Figure 5.*** $^{13}$C−$^{1}$H dip-shift NMR of nanodiamond and alanine at 4-kHz MAS and after 0.1-ms cross polarization. The normalized $^{13}$C signal intensity is plotted as a function the MREV-8 homonuclear decoupling time during which the $^{13}$C spin is subject to the $^{1}$H−$^{13}$C dipolar coupling. From top to bottom, data points are for the COO and $CH_3$ groups of alanine, the $CH_3$ group of alanine in 40-$\mu$s dipolar-dephasing difference spectra, the CH group in alanine (regular and dipolar-dephasing difference intensities coincide), and nanodiamond in dipolar-dephasing difference spectra. The dashed lines are guides to the eye.

this signal would match a sideband of the main alkyl peak at 35 ppm if the experiment was performed at 11.4 kHz MAS in their magnetic field of 14 T; this interpretation is supported by the lack of any other spinning sideband, which should be observed due to the combined chemical and paramagnetic shift anisotropies. Figure 3d−f demonstrates that sidebands of the band centered at 37 ppm can be clearly seen in the 100−150 ppm region under equivalent conditions. Unfortunately, ref 25 does not seem to report the spinning frequency used in their experiment, and an inquiry with the corresponding author was inconclusive. An alternative assignment would be to Teflon, $(CF_2)_n$, commonly used as a pliable spacer material in solid-state NMR, which is invisible in CP, but produces a peak at ∼111 ppm in DP experiments.

**Evidence of Protons Directly Bonded to Carbon.** Figure 4a presents the $^{1}$H spectra of nanodiamond at slow MAS (6.5 kHz). The width of the observed bands (>10 kHz) indicates a significant proton density on the surface. The narrow (2.6-kHz wide) signal reported by Panich et al.[25] and its interpretation as resulting from relatively isolated protons bonded to nanodiamond surface carbon in C−H and/or C−OH groups is not corroborated in our experiments, which employed probehead background suppression. Care must be taken to avoid absorption of water by the hygroscopic sample.[50,51] We also found that heating to remove water may lead to an alteration of the surface structure. The interference from mobile water can be circumvented by indirect detection of the $^{1}$H spectrum using $^{1}$H−$^{13}$C WISE with $^{13}$C decoupling during $^{1}$H evolution and short Lee−Goldburg cross-polarization, which provides a spectrum of the $^{1}$H bonded to $^{13}$C. The broad sideband pattern observed, Figure 4b, confirms that the sharp line reported by Panich et al.[25] is mostly not from surface-bonded protons.

The 30-kHz MAS spectrum, shown in Figure 4c, reveals that the $^{1}$H chemical shift is at 3.8 ppm, which is unusual for alkyl groups. The assignment to C−H, rather than $H_2O$, protons is confirmed by the cross peak between the 3.8-ppm $^{1}$H and 37-ppm $^{13}$C resonances in the $^{1}$H−$^{13}$C HetCor spectrum of Figure 4d; this spectrum was acquired with short LG-CP and is therefore dominated by signals of directly bonded $^{13}$C−$^{1}$H pairs. In addition, obvious spinning sidebands are observed in the $\omega_1$ dimension of the 2D HetCor spectrum (see Figure SI.1a), proving strong $^{1}$H−$^{13}$C dipolar couplings and thus close carbon−hydrogen proximity (for details, see the Supporting Information).

The strongly distance-dependent $^{13}$C−$^{1}$H dipolar coupling can also be probed by "dip-shift" NMR with dipolar-dephasing difference, as described in the Experimental Section. Since the signal of nonprotonated C contributed about one-fourth of the total intensity even after a short 0.1-ms CP time, the dipolar-dephasing difference approach was chosen, where the signal of nonprotonated C remaining after 40 $\mu$s of dipolar dephasing is subtracted out. The only slightly accelerated dephasing of the $CH_3$ signal of alanine, see middle traces in Figure 5, confirms that this procedure does not artificially produce a fast decay. For the CH group of alanine, the regular and the dipolar-dephasing difference signals do not differ significantly. Figure 5 shows that the dephasing of the alanine CH and nanodiamond dipolar dephasing difference signal are similar. In fact, faster dephasing in nanodiamond suggests a slightly larger one-bond C−H dipolar coupling, possibly due to reduced mobility of the relatively rigid diamond lattice. The data indicate a regular C−H bond of ∼0.11 nm length and exclude a structure proposed in ref 30 where the H atom is at a bridge site for two carbon atoms, with 0.15 nm C−H distances.

**Surface Carbons.** The DP/MAS $^{13}$C NMR spectrum of Figure 6a provides quantitative information on all carbons, and Figure

(50) Ji, S.-F.; Jiang, T.-L.; Xu, K.; Li, S.-B. *Appl. Surf. Sci.* **1998**, *133*, 231–238.
(51) Iakoubovskii, K.; Mitsuishi, K.; Furuya, K. *Nanotech.* **2008**, *19*, 1557051–1557055.

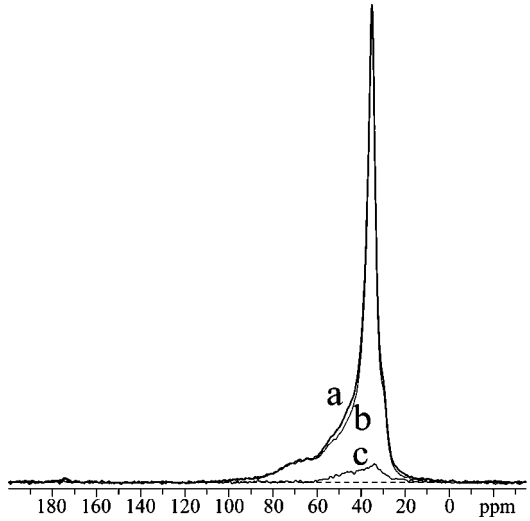


***Figure 6.*** Quantitative $^{13}C$ NMR spectra of nanodiamond, acquired after a Hahn echo at an MAS frequency of 14 kHz, with 5-s recycle delay. (a) Spectrum of all carbon. (b) Corresponding spectrum of quaternary carbons, obtained after 68 $\mu$s dipolar dephasing centered on the $^{13}C$ 180° pulse. (c) Difference spectrum obtained by subtracting (b) from (a), dominated by signals of protonated carbons.

6b displays the corresponding spectrum of nonprotonated carbons obtained under the same conditions but after a recoupled gated decoupling time of 68 $\mu$s. The difference of these spectra results in a spectrum dominated by signals of protonated carbons, shown as Figure 6c; it accounts for 6% of total carbons. Note that the chemical shifts of these 6% protonated carbons overlap with the chemical shift ranges of both the diamond core and the nonprotonated carbons in the disordered shell.

The elemental analysis indicates that ~14% of all C are part of CH or COH groups (and possibly some strongly adsorbed $H_2O$), and the first carbon layer of nanoparticles with a diameter of ~4.8 nm and a 0.1-nm layer spacing accounts for ~12% of all carbons.[18] From data shown in Figure 6c, we have found that 6% of all carbons are protonated (CH). This means that about half of the carbons at the nanodiamond surface are protonated. The rest is mostly bonded to OH groups (see below).

In order to obtain more detailed information on the surface carbons, we applied a series of spectral editing techniques. Carbons near protons can be observed selectively in $^1H-^{13}C$ CP NMR. Figure 7a shows the CP/TOSS spectrum with a contact time of 0.2 ms, selecting primarily signals from protonated carbons and some from nonprotonated carbons close to protons. Figure 7b shows the CP/TOSS spectrum with 0.2-ms CP and 40-$\mu$s dipolar dephasing, showing the nonprotonated carbons sufficiently close to protons. The difference of the two spectra is the spectrum of the protonated carbons ($CH_2$ + CH) shown in Figure 7c. All three spectra are plotted on an absolute intensity scale; the large band centered at 40 ppm is assigned to alkyl carbons, and the weak band at 70 ppm can be assigned to OCH carbons. The CH-only spectrum shown in Figure 7d demonstrates a similar, relatively symmetrical band around 40 ppm. No significant $CH_2$ signals were observed in $CH_2$-only spectra (not shown).

A band of COH groups is clearly observed near 72 ppm in the spectrum of Figure 7a,b. This is particularly interesting in view of the statement in a recent publication[29] that "...polarity has been thought to come from abundant C−OH groups... it is now clear that these are not due to C−OH but from adsorbed water". Our NMR data refute this claim and are consistent with

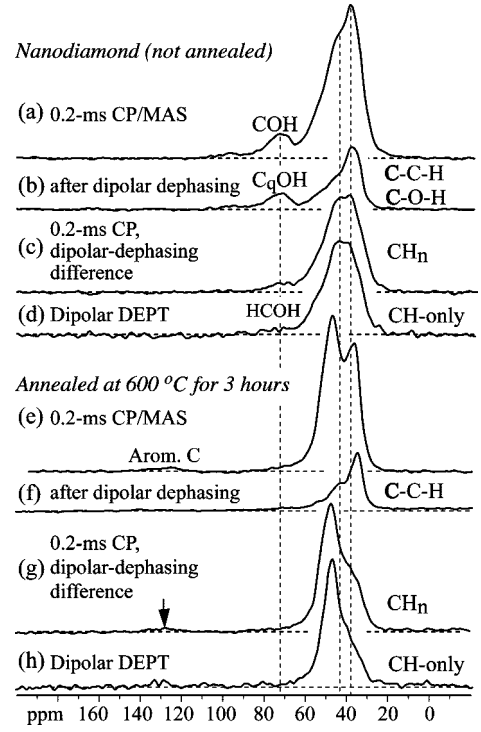


***Figure 7.*** Selective $^{13}C$ NMR spectra of surface and subsurface carbons, for (a−d) unannealed nanodiamond and (e−h) nanodiamond powder annealed at 600 °C under argon for 3 h. (a, e): Spectra of all carbon close to protons, obtained after 0.2-ms CP. (b, f) Spectra of the subsurface layer, obtained after 0.2-ms CP and 40-$\mu$s dipolar dephasing. (c, g) Spectra of protonated surface carbons ($CH_n$), obtained as the difference between the two preceding spectra. (d, h) Spectra of the CH (methine) groups, obtained by dipolar DEPT at 5787 Hz MAS.

the conclusion, from wear studies and DFT calculations, that dangling bonds at diamond surfaces will readily dissociate $H_2O$ to produce C−OH groups and bound H.[30]

**Comparison with Annealed Nanodiamond.** We also applied spectral editing to nanodiamond annealed by heating at 600 °C for 3 h under argon protection. For annealing at this temperature, Raman scattering shows an unexplained decrease in the intensity of the diamond bands, while significant graphitic signals are not yet observed.[28] While the direct polarization $^{13}C$ NMR spectrum shows relatively little change with annealing (not shown), the NMR results shown in Figure 7e−h reveal clear modifications in the surface structure after annealing. The disappearance of the signals observed at 70 ppm for the unannealed sample shows that annealing removes the OH groups from the nanodiamond surface. In addition, the chemical shift of the main protonated-carbon peak moved to higher field, see Figure 7e,g,h. The $CH_n$ spectrum, Figure 7g, shows that some CH signals appear at the $sp^2$ carbon position, marked by an arrow. These protonated aromatic carbons account for 3% of all C in the annealed sample.

**$^{15}N$ NMR.** Nanodiamond typically contains 2% nitrogen. Since N has one more electron than C, it produces a variety of defects in diamond. One of the simplest defects is single nitrogen substituting carbon, which results in an unpaired electron (formally on one of the neighboring carbons). [52] In EPR, such a defect produces a characteristic triplet due to the $2I + 1 = 3$ orientations of the $I = 1$ nuclear spin of $^{14}N$. However, for detonation nanodiamond, no significant triplet signal has been

(52) Jelezko, F.; Wachtrup, J. *Phys. Status Solidi* **2006**, *203*, 3207–3225.

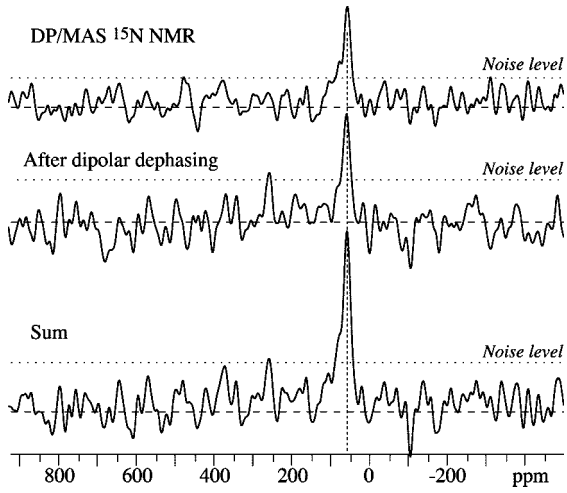


***Figure 8.*** Direct-polarization $^{15}$N NMR spectra of nanodiamond, at 6.5 kHz MAS. (a) Full spectrum. Measuring time: 5 days. (b) Spectrum after 0.3 ms of recoupled N−H dipolar dephasing. Measuring time: 3.5 days. The spectrum has been scaled to account for the different number of scans. (c) Sum of the spectra in (a) and (b) for improved signal-to-noise ratio. The approximate noise levels are indicated by dotted lines.

observed, excluding a significant fraction of single substitutional N.[21,53,54] The observability of nitrogen in the direct-polarization $^{15}$N NMR spectrum of nanodiamond shown in Figure 8 confirms this conclusion, since the signal of N next to an unpaired electron would be broadened beyond observability. Due to the small natural abundance of the $^{15}$N isotope (0.37%), the low abundance of N in nanodiamond (∼2%), and the small magnetogyric ratio of $^{15}$N, the sensitivity of $^{15}$N NMR is ∼2000 times smaller[55] than for $^{13}$C NMR of nanodiamond, and the observed signal intensity indicates that most $^{15}$N is detected. The observed ∼60-ppm chemical shift (relative to liquid $NH_3$ at 0 ppm) is in the range typical of tertiary amines, as expected. Possible structures without unpaired electrons are pairs of neighboring substitutional nitrogen atoms, or groups of four nitrogens around a vacancy.[52] The $^{15}$N spectrum and its short $T_1$ relaxation time also confirm that nitrogen is indeed incorporated into nanodiamond, contrary to speculations in ref 56.

DFT simulations have suggested that the lowest-energy sites for N in nanodiamond are at or near the surface.[18] To look for the resulting N−H at the surface,[18] we performed $^{15}$N NMR with 0.3 ms of recoupled dipolar dephasing before detection, which suppresses NH signals. The lack of any signal reduction in the resulting spectrum presented in Figure 8b (in fact, due to noise, the signal is slightly higher) shows that NH moieties are not common (<20%, given the limited S/N ratio). No $^1$H−$^{15}$N CP signal was observed either.

The presence of N in the diamond lattice can explain some of the nanodiamond $^{13}$C signal components shifted to higher frequency from the pure-diamond resonance position. Bonding of carbon to N usually results in a $^{13}$C shift of about +10 ppm, which affects the three carbons bonded to N in nanodiamond, i.e., 3 × 2% = 6% of all C. The next-nearest carbon neighbors

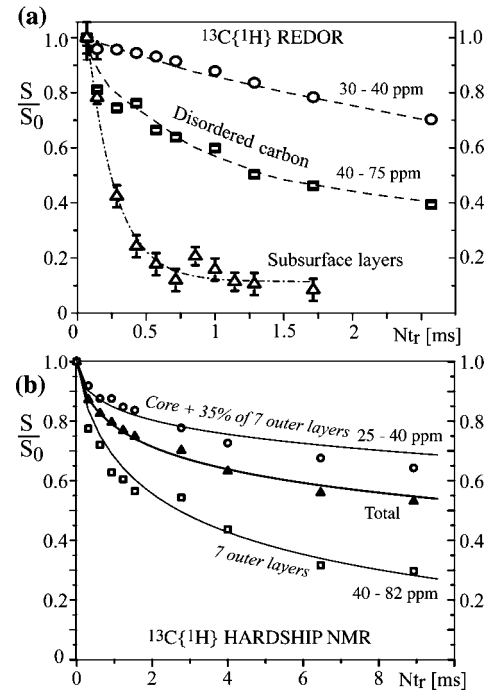


***Figure 9.*** $^{13}$C{$^1$H} dephasing in nanodiamond. (a) $^{13}$C{$^1$H} REDOR dephasing of nonprotonated carbons at 14 kHz MAS. Circles, core (30−40 ppm); squares, disordered carbon (40−75 ppm); triangles, subsurface carbon obtained after CP and dipolar dephasing. Dashed lines are guides to the eye. (b) $^{13}$C{$^1$H} HARDSHIP dephasing of all carbons at 6.5 kHz MAS, with fit curves. Circles, signal from 25 to 40 ppm; squares, disordered-carbon signal from 40 to 82 ppm; triangles, total signal from 25 to 82 ppm. Fit curves for 4.8-nm diameter nanodiamond particles, with seven outer layers of disordered carbon, 65% of which resonate within 40−82 ppm and 35% within 25−40 ppm, are also shown.

of N, which account for about 9 × 2% = 18% of all C, are also expected to be shifted by several ppm from the diamond $^{13}$C signal. As a result, almost a quarter of all C may experience a high-frequency shift due to nitrogen in the diamond lattice.

**Depth Measurements.** Given that only the surfaces of the nanodiamond particles are protonated, we can use $^1$H−$^{13}$C dipolar couplings to measure the depth of any spectrally resolved carbon site from the surface protons.

**REDOR Recoupled C−H dephasing.** The most commonly used pulse sequence for recoupling heteronuclear interactions is REDOR. We have demonstrated that its use for recoupled long-range C−H dephasing enables distinction of nonprotonated carbons at various distances from the nearest protons.[44] Figure 9a shows the recoupled C−H dipolar dephasing of nonprotonated nanodiamond carbons, with the intensity of the signal after 68 $\mu$s of dipolar dephasing normalized to unity. In the experiment with direct polarization, the carbons in the region of 30−40 ppm dephase more slowly than those between 40 and 75 ppm. This shows that the signals from 30 to 40 ppm represent predominantly the diamond core while those in the range of 40−75 ppm must be assigned to the outer shell of a given particle. The shoulder observed at 30 ppm in DP spectra of nanodiamond, for instance in Figure 1, dephases as slowly as the main peak and becomes better defined at longer dephasing times, which indicates that it is a component of the nanodiamond core. Its structural origin is not clear.

By using the recoupled C−H dipolar dephasing experiment after CP and 40-$\mu$s gated decoupling at 6.25 kHz MAS, we can selectively monitor the dephasing of nonprotonated carbons in the subsurface layers, since CP selects carbons near protons and

(53) Newton, M. E.; Baker, J. M. *J. Phys.: Conden. Matt.* **1989**, *1*, 9801–9803.
(54) Banaszak, A.; Fabisiak, K.; Kaczmarski, M.; Kozanecki, M. *Cryst. Res. Technol.* **2006**, *41*, 535–540.
(55) Harris, R. K. *Nuclear Magnetic Resonance Spectroscopy*; Longman: Harlow, U.K., 1983; p 236.
(56) Iakoubovskii, K.; Baidakova, M.; Wouters, B. H.; Stesmans, A.; Adriaenssens, G. J.; Vul, A. Y.; Grobet, P. J. *Diamond Relat.Mater.* **2000**, *9*, 861–865.

thus close to the surface. As expected, the data in Figure 9a show that the carbons in the subsurface layers decay the fastest since they are closest to protons.

**$^{13}$C{$^1$H} HARDSHIP NMR.** The REDOR data are difficult to analyze quantitatively, due to the effect of the strong $^1$H homonuclear couplings during the long heteronuclear dephasing.[48] We have shown that the HARDSHIP dephasing method avoids these difficulties by terminating a given period of heteronuclear dephasing before homonuclear effects become significant; this relatively short heteronuclear recoupling period is repeated many times to generate significant dephasing.[48] Figure 9b presents the dephasing of carbons using $^{13}$C{$^1$H} HARDSHIP NMR. Three sets of data points are shown—from signals within 25−40 ppm, within 40−82 ppm, and within 25−82 ppm (total with differential-$T_2$ correction; same data as shown in ref 48). The curves were simulated assuming 4.8-nm diameter particles with 60% C−H and 40% O−H groups at the surface. The simulation results indicate that there are seven outer carbon layers with a thickness of 0.63 nm contributing to the signal between 40 and 82 ppm, and that 35% of the seven outer layers resonate in the 25−40 ppm range, overlapping with the core-carbon peak. The thickness of the partially disordered layer is quite consistent with a recent simulation of small nanodiamond grains, where the thickness of the structurally disturbed surface layer was ∼0.5 nm.[18]

**Unpaired Electrons in Nanodiamond.** In magnetic measurements, it has been found that a ∼4.6-nm diameter nanodiamond grain contains ∼30 unpaired electrons (or 35 electrons in a 4.8-nm particle) on average.[57] As mentioned above, in the EPR spectrum of detonation nanodiamond the triplet characteristic of the $^{14}$N nuclear spin is not observed. This shows that the unpaired electrons are mostly not due to N, but bonding defects in the carbon lattice.[21,53,54] We have observed the effects of the electron spins on the NMR relaxation times and analyzed the longitudinal relaxation quantitatively as described in the following.

**Invisible carbon near unpaired electrons.** Due to thermal averaging, the effective "Curie" spin $S_c$ of an unpaired electron in nanodiamond is given by

$$S_C = \frac{-\gamma_e \hbar S(S+1)B_0}{3kT} \tag{2}$$

where $\gamma_e$ is the gyromagnetic ratio of the electron ($-1.76 \times 10^{11}$ s$^{-1}$ T$^{-1}$ = 658.5 $\gamma_{1H}$), $\hbar$ is Planck's constant/$2\pi$, $S$ the electron spin quantum number (1/2), $B_0$ the magnetic field, $k$ the Boltzmann factor ($1.38 \times 10^{-23}$ J/K), and $T$ the absolute temperature.[58] Under our experimental conditions, with $B_0$ = 9.4 T and $T$ = 293 K, we obtain $S_C = -0.011$. Comparing with the full $S$ = 1/2, this means that the electrons are 2.2% polarized.

Due to the thermal averaging of the electron spin $S_Z$ to the Curie spin $S_C$, the effect of the electron−nuclear Hamiltonian is reduced to that of a $B$-field with the strength of the dipolar coupling constant and can be expressed as follows[58]

$$\delta_{PSA} = \frac{-\mu_0 \hbar \gamma_e \gamma_{^{13}C}}{4\pi r^3} 2S_C = -S_C 2\pi 39.5\text{MHz}\frac{\text{Å}^3}{r^3} \tag{3}$$

The field-proportional and orientation-dependent coupling in eq 3 behaves essentially like a chemical-shift anisotropy (CSA), and is referred to as the paramagnetic-shift anisotropy (PSA).[59,60] At $T$ = 293 K, for distances >0.3 nm we find $\delta_{PSA}$ < 15 kHz, which is sufficiently small for the signal to be mostly observable. At shorter electron−carbon distances, the intensity of the carbon centerband is strongly reduced. With an unobservable volume of $35 \times 4/3\pi\ (0.3\ \text{nm})^3 = 4\ \text{nm}^3$ around the 35 unpaired electrons and a total nanodiamond particle volume of $4/3\pi$ (4.8/2 nm)$^3$ = 58 nm$^3$, less than 8% of carbon is not observable.

**Fast $T_{1,C}$ Relaxation.** Combining $^{13}$C DP- or CP-REDOR with $T_1$ relaxation measurements, $T_1$ relaxation of core and shell carbons can be measured quite selectively. The nanodiamond $^{13}$C $T_1$ ($T_{1,C}$) relaxation curves of carbons directly bonded to hydrogen, in the subsurface layers, in the whole disordered shell, and in the core are shown in Figure 10a. Long-range $^1$H−$^{13}$C dipolar dephasing did not change the $T_{1,C}$ curve of the core carbon signal significantly (not shown). For reference, the $T_{1,C}$ relaxation curves of natural and synthetic microdiamonds are also plotted in Figure 10a. The $T_{1,C}$ values of all parts of nanodiamond are within 1 s, compared to hundreds of seconds for micrometer-size diamonds. In addition, the relaxation curves in nanodiamond are nonexponential. Both observations indicate the presence of unpaired electrons.

Electron $T_1$ relaxation produces a fluctuating field at the $^{13}$C nucleus that drives its longitudinal ($T_{1,C}$) relaxation. $T_{1,C}$ is strongly dependent on the distance $r_n$ between a given carbon and the $n$th unpaired electron:

$$1/T_{1,C} = A^{-1} \sum_{n_{electron}} 1/r_n^6 \tag{4}$$

where the prefactor $A^{-1}$ depends on the longitudinal relaxation time $T_{1,e}$ of the unpaired electrons, as detailed in ref 58. In Figure 10a the $T_{1,C}$ of the disordered shell is shorter than that of the surface or of the core, indicating that disordered carbons are closer to unpaired electrons. It is particularly interesting to note the $T_{1,C}$ of carbons in the surface and subsurface layers is longest, which was seen consistently in both CP and DP dipolar-dephasing difference experiments (latter not shown). This combination of spectral editing with $T_{1,C}$ measurements indicates that the ad-hoc assignment of the short $T_{1,C}$ component to surface carbons proposed in ref 25 is incorrect. This observation also shows that the unpaired electrons are not due to dangling bonds on the surface. For quantitative confirmation, Figure 10b shows a simulation of the relaxation curves for a model nanodiamond grain with 35 unpaired electrons present as dangling bonds in the outer 0.2 nm of the spherical particle of 4.8-nm diameter. As expected, the relaxation for the core (plus 35% of the shell carbon, which overlaps) in this dangling-bond model is significantly slower than that of the shell or the surface layer, contrary to the experimental observation. In order to preempt potential concerns, carbons within 0.6 nm from the unpaired electron were considered as unobservable; with a smaller unobservable radius, the contrast between core and shell relaxation would be even larger. The absence of a significant fraction of unpaired electrons at the surface is consistent with EPR studies that did not show any significant change in EPR signal with chemical modification (chlorination, methylation, etc.) of the nanodiamond surface.[61]

The data in Figure 10a can be fitted with a model where unpaired electrons are found at depths between 0.4 and 1 nm from the particle surface. The value of $A$ in eq 4 was set to 3.5

(57) Levin, E. M.; Fang, X.-W.; Bud'ko, S. L.; Straszheim, W. E.; McCallum, R. W.; Schmidt-Rohr, K. *Phys. Rev. B* **2008**, *77*, 0544181−05441810.
(58) Gueron, M. *J. Magn. Reson.* **1975**, *19*, 58–66.
(59) Bertini, I.; Luchinat, C. *Coord. Chem. Rev.* **1996**, *150*, 29–75.
(60) Antonijevic, S.; Persson, E. *J. Chem. Phys.* **2007**, *126*, 0145041−0145047.
(61) Belobrov, P. I.; Gordeev, S. K.; Petrakovskaya, E. A.; Falaleev, O. V. *Dokl. Phys.* **2001**, *46*, 459–462.

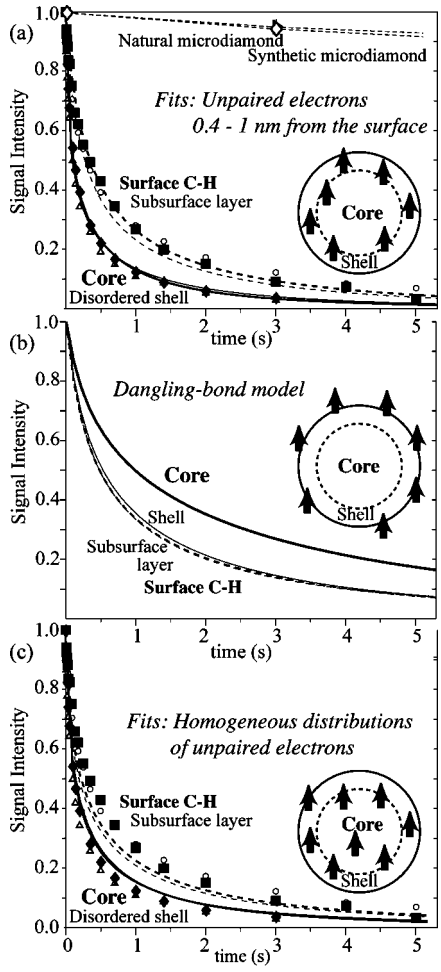


***Figure 10.*** $T_{1,C}$ relaxation data for nanodiamond measured at 6.25 kHz MAS, with simulation curves. (a) Filled squares: carbon directly bonded to H; open circles: subsurface layer (from dipolar-dephasing difference after cross polarization); filled diamonds: core (25−47 ppm); open triangles: disordered carbon (47 −85 ppm). The $T_1$ relaxation curves of two microdiamond samples are shown for reference at the top. Simulated fit curves are for a model with 40 unpaired electrons per particle, at depths between 0.4 and 1 nm from the surface. Curves for the surface and the first subsurface layer are shown by thick and thin dashed lines, respectively, those for the core and shell by continuous thick and thin lines, respectively. (b) Simulated relaxation curves for a model with dangling bonds, unpaired electrons at the particle surface. The relaxation is slowest for the core, contrary to the experimental data in (a). (c) Simulated relaxation curves for a homogeneous distribution of unpaired electrons, with the data points from (a) superimposed.

s/nm$^6$, and carbons within 0.3 nm from the unpaired electrons were treated as unobservable. The spherical particle contained 40 unpaired electrons, consistent with recent magnetic analyses of the same material.[57] At a lower number of electrons per particle, the depth dependence of the relaxation curves is less pronounced than observed experimentally because with few electrons in the particle, large portions of the layers that can contain unpaired electrons are actually free of unpaired electrons. The distribution of depths (0.4−1 nm) of the unpaired electrons from the particle surface is directly reflected in the multimodal relaxation of the carbons in the surface layer. The fraction of unpaired electrons near (∼0.4 nm from) the particle surface is also crucial for making the relaxation of the carbons in the core slower than that of the shell carbons, since they affect the core less than the shell. For a model with a distribution of electrons throughout the whole particle, the difference between the relaxation curves is too small, see Figure 10c, as should be expected. While for a fully homogeneous distribution of electrons, all relaxation curves would coincide, the surface carbons in this model still relax slightly slower than those in the core since even with unpaired electrons in six neighboring particles included in the simulation, the concentration of unpaired electrons outside the particle is still lower than inside.

**Chemical-Shift Dispersion.** The 5−30 ppm chemical shift of ∼50% of all C in nanodiamond from the regular diamond resonance is considerable. Such shifts may occur due to proximity of C to H, O, or N, or to defects in the diamond lattice. About 30% of all carbons are within three bonds from H and O at the particle surface, and ∼24% are within two bonds from one of the ∼200 N per particle (see above). Some paramagnetic shift due to the unpaired electrons, as well as chemical shift due to lattice distortions near their associated defects, is also to be expected. The shell may also contain a significant number of defects that are not paramagnetic.[54] It is interesting to note that both experiments[62] and ab initio calculations[63] show a ∼70-ppm chemical shift for amorphous sp$^3$-hybridized carbon. In this context, it should also be noted that the 37-ppm chemical shift of neat diamond cannot be understood in terms of standard substitution rules for alkyl carbons,[64] which predict a value >50 ppm, but has been reproduced in ab initio calculations.[63]

**Comparison with Previous Models.** Several nanodiamond structural models have been proposed in the literature, such as the bucky-diamond model,[18,24] a model featuring an aromatic onion shell,[20,21] and a hollow-center model.[22] For a nanodiamond grain with a diameter around 4.8 nm, the first carbon layer accounts for 12% of all carbons. Since less than 1% is from sp$^2$-hybridized carbon (Figure 3), and no "onion shell" diffraction peak at 13° is seen in the X-ray diffraction pattern (Figure 2), we can clearly rule out the fullerenic and onion shell surface models. [18,20−22,24,25] Note that no significant signal of sp$^2$-hybridized carbons was observed in any of the previous NMR studies of purified nanodiamond[7,10,25,36] the peak at 111 ppm in the widely quoted[29] ref 25 is not at the expected ∼130-ppm resonance position[62] and is most likely an artifact, as discussed above. Consistent with our results, studies of diamond coatings structurally perturbed by wear and corresponding DFT simulations have concluded that passivation of dangling bonds by reaction with $H_2O$ or $H_2$ occurs in preference to graphite formation.[30,31] A matrix of soot structures covering the surface of agglomerates of several nanodiamond particles[4,29] is also excluded by our results. Just a monomolecular layer of aromatic rings at the particle surface would contain ∼10% of all C in the material, far above our detection limit.

Fast C−H dephasing and strong dipolar sidebands in 2D HetCor spectra show that many of the surface carbons are directly bonded to protons, while others are part of COH groups. In turn, the $^{13}C\{^1H\}$ REDOR and HARDSHIP results confirm that the ordered diamond carbons are far from the protons, i.e., in the core, while the disordered sp$^3$-hybridized carbons are closer to the surface. The $T_{1,C}$ experiments indicate that unpaired electron are located at an intermediate depth, not in the center, and also not as dangling bonds on the surface. The hollow center

(62) Alam, T. M.; Friedmann, T. A.; Schultz, P. A.; Sebastiani, D. *Phys. Rev. B* **2003**, *67*, 2453091:11.
(63) Mauri, F.; Pfrommer, B. G.; Louie, S. G. *Phys. Rev. Lett.* **1997**, *79*, 2340–2343.
(64) Bovey, F. A.; Jelinski, L.; Mirau, P. A., *Nuclear Magnetic Resonance Spectroscopy*, 2nd ed.; Academic Press: San Diego, 1988.

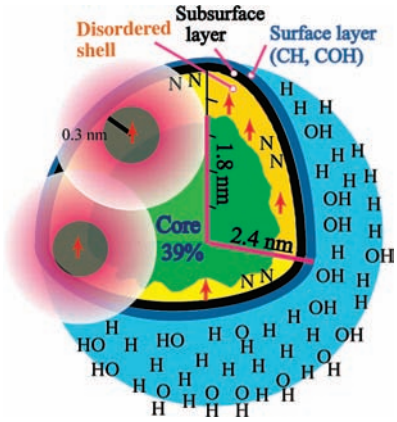


***Figure 11.*** Schematic model of the structure of nanodiamond. The hydrogenated surface is part of a 0.6-nm-thick shell of seven partially disordered carbon layers that contain 61% of all C and mostly produce higher-field $^{13}$C NMR signals. Unpaired electrons (indicated by red arrows) occur with a density of ~40 per particle and are located 0.4−1 nm from the surface. About 8% of all carbon are within 0.3 nm from the unpaired electron and thus unobservable by NMR.

structural model is also not suitable for our detonation nanodiamond sample because no sp$^2$ carbons are observed and $T_1$ of core carbon is longer than the $T_1$ of other carbon species.

**NMR-Based Model of Nanodiamond.** Figure 11 displays the nonaromatic core−shell model of detonation nanodiamond developed based on our experimental NMR results. The nanodiamond particle has a diameter of 4.8 nm and contains close to 10 000 carbon and 200 nitrogen atoms.[65] The nanodiamond surface carbons are bonded to H and OH groups. Only 39% of carbons are in the 3.6-nm diameter ordered diamond core; 40% of carbons are in a five-layer-thick, partially disordered shell containing unpaired electrons; and additional 21% carbons are located in the two outermost carbon layers. The thickness of the partially disordered shell is around 0.63 nm. The crystalline core diameter of 4 nm deduced from WAXD includes the ordered core and some ordered regions in the partially disordered shell. Unpaired electrons are located mostly in the disordered shell, at distances of 0.4−1 nm from the surface, with a density of ~40 unpaired electrons per 4.8-nm diameter particle. The fraction of carbon that is unobservable due to close proximity (<0.3 nm) to an unpaired electron is <8%.

A partially disordered shell of 0.5−0.7 nm thickness containing sp$^3$-hybridized carbon has been generated or postulated in some simulations of hydrogen-terminated nanodiamond,[18,66,67] while simulations for extended hydrogenated diamond crystals find only a reconstruction of the 0.2-nm-thick surface layer.[68] Barnard and Sternberg found a 0.5-nm-thick disordered layer in DFT simulations aimed at identifying the energetics of nitrogen in nanodiamond.[18] Palosz et al. have postulated a 0.7-nm-thick strained shell for SiC and nanodiamond particles, based on considerations of surface tension and surface curvature preventing a simple reconstruction of the surface layer. [66,67] A noncrystalline core−shell model has also been proposed based on parallel electron-energy-loss spectra of nanodiamond (PEELS) spectra.[69] However, the shell in these models is around 3.8-nm-thick and accounts for >85% of all carbons, which is rather different from our findings.

## Conclusions

We have studied synthetic nanodiamond with a crystalline core of ~4-nm diameter. Short $^1$H−$^{13}$C dipolar dephasing shows that about 6% of all carbons, about half of surface sites, are protonated, while the other half are bonded to OH groups that are mostly removed by annealing at 600 °C. No aromatic carbons were found, ruling out fullerenic or graphitic surface layers in the two samples studied. A scattering feature previously attributed to graphitic onion shells was not observed here and shown to be most likely an artifact of a plastic sample holder. $^1$H NMR and $^{13}$C{$^1$H} HetCor consistently showed an unexpected 3.8-ppm chemical shift position of the surface protons; the protons were proved to be bonded to carbons (rather than O in −OH or $H_2O$) by fast C−H dipolar dephasing and strong $^{13}$C−$^1$H dipolar sidebands in HetCor spectra. Most nitrogen, detected in direct-polarization $^{15}$N NMR spectra, is not protonated and therefore not at the particle surface. Given the protonated surface, $^1$H−$^{13}$C HARDSHIP NMR can probe the depth of various sites from the surface. The higher-frequency signals dephased faster than the ideal-diamond carbon signal, corroborating the assignment of the broad higher-frequency bands to a disordered shell of ~0.63 nm thickness, in a particle of 4.8 nm diameter. Fast $T_{1,C}$ relaxation (<1 s) observed for all carbons in nanodiamond is due to interactions with ~40 unpaired electrons per grain. The longer $T_{1,C}$ of the protonated surface carbons and the layer underneath prove that most unpaired electrons are not from dangling bonds at the surface but from unpaired electrons at depths of 0.4−1 nm. Our study should serve as a benchmark for future investigations of other types of nanodiamond,[2] including those in meteorites or made by chemical vapor deposition (CVD) synthesis.[6] Further theoretical studies are needed to explain the formation of the observed disordered shell containing nitrogen and unpaired electrons, in terms of the high-temperature and pressure processes during nanodiamond formation.

**Acknowledgment.** This work was supported by the National Science Foundation (Grant No. CHE-0138117). The authors thank Zhihong Tang for help with preparing the annealed nanodiamond sample.

**Supporting Information Available:** Analysis of dipolar spinning sidebands in $^1$H−$^{13}$C HetCor NMR spectra. This material is available free of charge via the Internet at http://pubs.acs.org.

JA8054063

(65) Jones, A. P.; d'Hendecourt, L. *Astron. Astrophys.* **2000**, *355*, 1191–1200.
(66) Palosz, B.; Grzanka, E.; Gierlotka, S.; Stel'makh, S.; Pielaszek, R.; Bismayer, U.; Neuefeind, J.; Weber, H.-P.; Proffen, T.; Von Dreele, R.; Palosz, W. *Z. Kristallogr.* **2002**, *217*, 497–509.
(67) Palosz, B.; Pantea, C.; Grzanka, E.; Stelmakh, S.; Proffen, T.; Zerda, T. W.; Palosz, W. *Diamond Relat. Mater.* **2006**, *15*, 1813–1817.
(68) Kern, G.; Hafner, J. *Phys. Rev.B* **1997**, *56*, 4203–4210.
(69) Fehlhaber, R. P.; Bursil, L. A. *Phil. Mag. B* **1999**, *79*, 477–489.